Available online at www.sciencedirect.com

ScienceDirect

Procedia CIRP 31 (2015) 489 – 495

www.elsevier.com/locate/procedia

15th CIRP Conference on Modelling of Machining Operations

Modelling and Experimental Investigation of Cutting Temperature when Rough Turning Hardened Tool Steel with PCBN Tools

V. Kryzhanivskyy[1], V. Bushlya[2]*, O. Gutnichenko[2], I.A. Petrusha[3], J.-E. Ståhl[2]

[1]*Department of Computer Sciences, Zhytomyr State Technological University, Cherniachivskiy 103, Zhytomyr, 10013, Ukraine*
[2]*Division of Production and Materials Engineering, Lund University, Ole Römers vag 1, Lund, 22100, Box-118, Sweden*
[3]*Department of Sinthesis and Sintering of Superhard Materials, Institute for Superhard Materials, Avtozavodska 2, 04074, Kyiv, Ukraine*

* Corresponding author. Tel.: +46-046-222-4607; fax: +46-046-222-8504. *E-mail address:* Volodymyr.Bushlya@iprod.lth.se

Abstract

In this study the cutting tool temperature that develops during rough turning of hardened cold-work tool steel is modelled on the basis of experimental data. The data obtained from a series of thermocouples, placed on a PCBN insert, into an anvil, and into a toolholder, were used as the input for the model. An inverse problem was solved, where the heat fluxes and heat transfer coefficients were computed and where the developed temperature field was reconstructed from the experimental readings. The temperature was modelled for the case of new tools, as well as for the case of its development in the course of tool wear. The machining case involved utilization of a high-cBN content and a binderless PCBN grade, both possessing high thermal conductivity of 110 and 190 W/m K respectively.

Peer-review under responsibility of the International Scientific Committee of the "15th Conference on Modelling of Machining Operations

Keywords: Tool temperature; inverse problem; hard turning; PCBN

1. Introduction

The temperature that develops in the cutting process has a significant effect on the performance of a cutting tool and the quality of the machined component [1]. Such effects are especially accentuated when cutting difficult-to-machine materials like hardened steel, superalloys, titanium alloys, etc. High speed and thus economic machining of these workpiece materials requires utilization of polycrystalline cubic boron nitride (PCBN) tools since they retain their strength and hardness at high temperatures generated during the process [2]. At the same time high cutting temperatures create limitations to the tool performance due to chemical and diffusional wear of PCBN [3-5]. This emphasizes the need for accurate, easy, and reliable methods for the measurement of the temperature and especially its distribution on the tool surfaces and in the tools.

A large number of techniques for temperature measurement in machining, from dynamic thermocouple [6] to optical fiber [7, 8] and IR-CCD [3, 9, 10] imaging, that differ in complexity, accuracy, spatial resolution, cost, etc. are utilized [1]. Application of embedded thermocouples offers the ease of set-up, low cost, reasonably fast response but a low spatial resolution in measurement. Ren et al. [11] utilized the combination of FE modelling and the use of a thermocouple on tool/shim interface in order to model temperature field in a PCBN tool and thus increase resolution of the data. The model however assumed a fixed and constant tool-chip temperature on the tool rake. El-Wardany et al. [12] also used the mixed FEM-experimental method but developed a complex and sophisticated calibration procedure to cope with the issue of temperature averaging on the tool-chip contact. Another approach to the modelling of the temperature distribution in a tool is to determine the heat flux into the tool from the chip and workpiece side [1]. Norouzifard et al. [13] utilized the embedded thermocouples for the estimation of the flux of the frictional heat into the tool and the chip by solving an inverse problem.

This article reports on the approach combining FE modelling with registration of a temperature in several locations on a tool. An inverse thermal solution was used for the determination of heat fluxes into the tool through the tool-chip and tool-workpiece interfaces and for the estimation of heat transfer coefficients between different materials in

Peer-review under responsibility of the International Scientific Committee of the "15th Conference on Modelling of Machining Operations
doi:10.1016/j.procir.2015.03.079

toolholder assembly and the environment. The obtained data are used for the reconstruction of temperature field in two PCBN grades used for machining hardened PM tool steel.

2. Experimental setup

The experimental machining operation included dry rough turning of hardened (HRC 58) tool steel Vanadis 4E (Uddeholm Tooling). Vanadis 4E is a powder metallurgy cold work tool steel. Cutting conditions were kept constant: $v_c = 70$ m/min, $f = 0.5$ mm/rev, and $a_p = 1$ mm. Two PCBN grades having high-cBN content were used in the tests. Binderless cBN (BCBN) possessing thermal conductivity of $k \approx 190$ W/(m·K) and an AlN, WB_2-bound CBN500 grade (SECO Tools) having $k \approx 110$ W/(m·K). Thermal conductivity at room temperature was determined by transient plane source method on IT3-MChTI device and on a hot disk TPS 2500 S analyser for BCBN and CBN500 grades respectively. Chamfered round inserts RNGN090300S-02020 were used in the tests. A neutral toolholder CRDNN3225P12 was used to ensure the centered positioning of the "tool-chip" contact zone with respect to the toolholder axis. A set of channels of 0.4×0.4 mm were cut on a precision diamond disk saw in the holder itself, in the cemented carbide anvil and in the cemented carbide clamp plate, all in the center-line direction of the toolholder. Two ∅ 0.5 mm holes were drilled in the holder, their dead-end being also located on the toolholder's center-line. Eight K-type thermocouples (TC1…TC8) were placed in the channels and holes according to the schematic drawing shown in Fig 1.

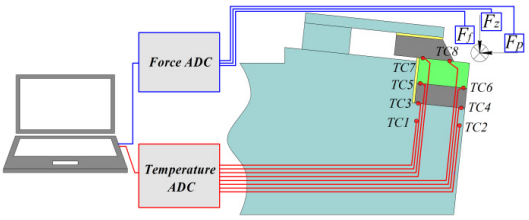

Fig. 1. Schematic view of the measurement system.

Fine gauge Kapton insulated thermocouples (Omega Engineering) SC-KK-K-40-1M with the wire diameter of 80 µm were used for the temperature registration in respective positions (Fig. 1). A silver thermal paste, having $k = 25$ W/(m·K), was applied on the interfaces, with thickness of 50 to 70 µm, and was filled into the channels to ensure proper contact conditions following the recommendations [1]. A paper gasket was used on the cylindrical surfaces of a PCBN insert and the anvil because they both have only a two-point contact with the toolholder which cannot be described mathematically in a correct way. For the same reason another paper gasket was used between the cemented carbide clamp plate and the cast steel clamp (Fig. 1). The temperature in the cutting tool was measured during the entire tool engagement of about 200 seconds and after tool disengagement for 400 seconds. Cutting forces were also recorded (Fig. 1 and 4) with the help of Kistler 9129AA three-axis piezoelectric dynamometer. 3-D geometrical analysis and crater measurement on the worn tools was done on the white light optical microscope InfiniteFocus Real3D, Alicona.

3. Modelling

The aim of modelling was to develop a mathematical model which allows reconstructing the temperature distribution in the tool in a good agreement with the experiments by solving an inverse problem. Computation of a temperature field in a given domain requires a solution of the boundary value problem for the heat equation. In mathematical terms, these problems are well studied and a number of computational tools for their solutions are readily available. However in an applied calculation the problem of determining the correct input data for the boundary value problem exists. In particular, the heat transfer coefficients (h_i) for the exchange with the environment and values of the heat fluxes (q_i). The knowledge of the total power consumed in the cutting process allows the estimation of the upper and lower limits of heat flux values. The upper and lower limits of heat transfer coefficients were taken for the case of solid-to-air free convection [14]. The determination of the exact values of the model input data of h_i, q_i becomes a problem of mathematical programming, where the maximum of squared difference between the modelled and experimental data in the points of interest is used as the objective function of the problem. The variables in the objective function are the values of heat fluxes q_i and heat transfer coefficients h_i. Minimum of the objective function on the feasible set of values of its variables, which is determined by their upper and lower limits, is the solution to the problem.

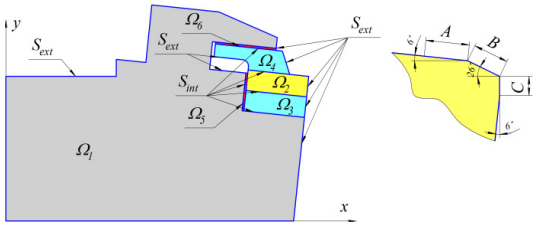

Fig. 2. Schematic of the computational model.

During the experimental measurements, all the thermocouples (TC1…TC8) were placed in the same plane. This allows the use of a two-dimensional model for the numerical calculations. The schematic of the computational model is shown on the Fig. 2. Geometrically, the system consists of six subdomains Ω_i, i=1…6, defined in the coordinate system xy. The subdomains have different thermal properties of the materials. Table 1 shows the materials of the subdomains and their thermal and physical properties.

High-temperature dependencies of the thermal properties for the materials in the subdomains were evaluated from the published literature. Thermal conductivity of PCBN $k(T)$ was extrapolated from room temperature values according to [15-17]. Data for the specific heat of PCBN grades $C_p(T)$ was taken from [18]. Data for both thermal properties $k(T)$ and $C_p(T)$ of cemented carbide were taken from [19]. Thermal properties for steel and paper were kept constant because of their slight variation in the studied temperature range.

Table 1. Material properties at room temperature [14]

Material	Subdomain	ρ, kg/(mm^3)	C_p, J/(kg·K)	k, W/(mm·K)
BCBN	Ω_2	3.4e-6	680	190e-3
CBN500	Ω_2	3.5e-6	640	110e-3
Steel	Ω_1	7.8e-6	470	44e-3
WC-10Co	Ω_3, Ω_4	14.6e-6	205	85e-3
Paper	Ω_5, Ω_6	0.8e-6	1340	0.8e-3

Inside every subdomain the balance relationship is satisfied as a result of the law of conservation of energy. In the differential form, this relationship equals:

$$\rho_i C_{pi} \frac{\partial u_i}{\partial t} - div\left(k_i \, grad\, u_i\right) = 0 \qquad (1)$$

where ρ_i, C_{pi}, k_i, $u_i(x,y,t)$, t – density, specific heat, thermal conductivity, temperature distribution, and time in the subdomain Ω_i respectively. Equation (1) has an infinite number of solutions. The boundary and initial conditions should be applied in order to obtain a solution that corresponds to the experimental conditions. A constant temperature of 20 ºC for all subdomains was selected as the initial condition: $u_i(x,y,0) = 20$, $i = 1,\ldots,6$.

The boundary conditions for each of the subdomains are divided into two types:

1. Boundary between adjacent subdomains S_{int} (Fig. 2).
2. Boundary of a subdomain with environment S_{ext} (Fig. 2).

A compatibility conditions between the subdomains Ω_i and Ω_j must be fulfilled at a boundary S_{int}:

$$u_i(x,y,t)\big|_{S\,\mathrm{int}} = u_j(x,y,t)\big|_{S\,\mathrm{int}}, \; k_i \frac{\partial}{\partial n} u_i(x,y,t)\Big|_{S\,\mathrm{int}} = k_j \frac{\partial}{\partial n} u_i(x,y,t)\Big|_{S\,\mathrm{int}}$$

where n – normal to S_{int}.

In turn, the exterior boundary is divided into sections where the heat exchange with the environment is proportional to the temperature of the subdomains and sections through which the heat is transferred from the cutting zone into the tool body. The boundary conditions on the exterior sections, which are describing the heat exchange with the environment, have the form:

$$n k_i \, grad\, u_i + h_i u_i\big|_{Sext} = 0 \,,$$

where n – normal to S_{ext}, h_i – heat transfer coefficient.

The conditions on the sections of the boundary corresponding to the tool-chip contact on the rake face (sections A and B) and to the tool-workpiece contact on the flank (section C) of the cutting tool (Fig. 2) are:

$$n k_2 \, grad\, u_2\big|_{A\,or\,B} = q_{rake} \,, \; n k_2 \, grad\, u_2\big|_C = q_{flank}$$

where q_{rake} and q_{flank} – the fluxes on the rake and the flank. The heat flux on both the rake and the flank surfaces was assumed to be uniform along the contact zone on the tool. It is known that the tangential stresses on the tool surfaces that are responsible for the frictional heat generation have a non-uniform distribution [20]. On the other hand experimental studies [21] indicate that the heat flux on the tool rake has a close to uniform distribution.

As mentioned above, the upper and lower limits of the fluxes q_{rake} and q_{flank} can be estimated from the total power consumed during cutting. The total power generated by the machining process is defined as a product of the cutting speed and the cutting force $P_c = F_c \cdot v_c$. It is known [14] that this P_c power is consumed in the primary, secondary, and tertiary deformation zones and only fractions of these individual powers reach the cutting tool because some parts remain in the chip and the machined workpiece (Fig. 3).

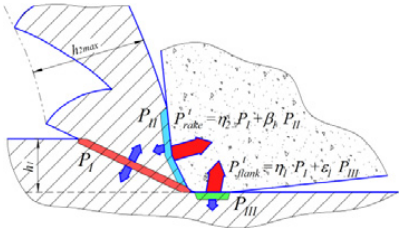

Fig. 3. Power consumption and power balance in the cutting process.

Therefore P_c is used only as the upper limit for the model. According to Fig. 4 the cutting force is similar for both PCBN grades and in unworn state equals to F_c=1950 N which corresponds to P_c=2.26 kW. The maximum possible heat flux through the rake face equals $q_{rake}^{\max}$ =1.44 kW/mm^2, when accounting for the average tool-chip contact length on the rake l_{rake} = 0.46 mm (Fig. 11) and the active length of the cutting edge L = 3.39 mm. Lower heat flux on the rake is expected in machining due to the influence of heat partition coefficient.

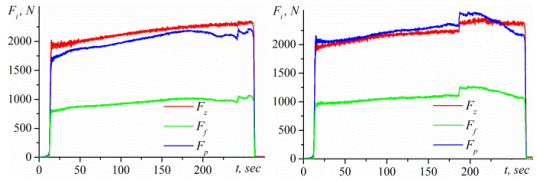

Fig. 4. Cutting forces for (a) BCBN and (b) CBN 500 tools.

An increase in the force during the tool engagement was attributed in the model solely to the development of the wear land VB. Reduction of the force acting on the rake associated with the development of the crater was not modelled because the cutting force F_c only slightly depends on the effective rake angle in the geometry range studied [22]. The force increment ΔF_c associated with the observed flank wear VB=0.43 mm for both PCBN tools equals ΔF_c = 410 N and respective ΔP_c=0.48 kW. Therefore the maximum possible heat flux through the tool flank equals $q_{flank}^{\max}$ =0.3 kW/mm^2.

The behavior of the fluxes on the tool rake and flank is modeled differently. On the rake face the flux remained constant and the sections A and B (Fig. 2) remained unchanged during the entire cutting process. On the flank at time t = 0 sec, the length of section C equals to the edge radius of the insert $C = r_\beta$ = 0.015 mm. With the onset of the tool wear during the cutting process, the length of the section C increases proportionally to its maximum value of VB = 0.43 mm. The contact length C developing in time is

calculated as $C = r_\beta + t\cdot(VB - r_\beta)/200$, where 200 sec is the modeling time. As a result, the flux through the flank is increased as a function of time according to $q_{flank} = P_{flank}/(C\cdot L)$, where P_{flank} is a part of power transferred to the tool through the flank (Fig. 3), L – active edge length measured perpendicular to the plane xy.

Table 2. Upper and lower limits for the model variables.

q_{rake}, W/mm^2		q_{flank}, W/mm^2		h_1, $W/(m^2K)$		h_2, $W/(m^2K)$		h_3, h_4, $W/(m^2K)$		h_5, h_6, $W/(m^2K)$	
min	max	min	max	min	max	min	max	min	max	min	max
0	1440	0	307	2	12	2	12	2	12	2	12

In the above formulation the obtained mathematical model depends parametrically on the fluxes on the tool rake and the flank, as well as the heat transfer coefficients at the external boundaries. Based on this formulation a finite element model of the process of heat distribution in the tool was created, in which these uncertain data were included as parameters. The modeling and calculations were performed with MATLAB®. Triangular mesh was obtained using a Delaunay triangulation algorithm (Fig. 5). The mesh growth rate away from finer parts of the geometry is equal to 30%. For the tool holder, where the temperature gradients are not significant, a coarser mesh was used to reduce processing time. A refined mesh is applied to the insert itself and adjoining zones of the anvil, clamp and clamp plate to increase calculation accuracy.

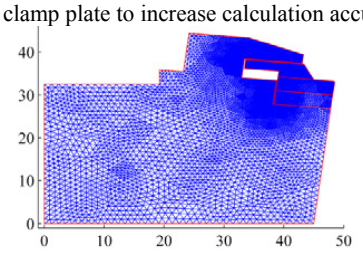

Fig. 5. FE model of the toolholder assembly and meshing method.

Such parametric representation of the FE model made it possible to formulate the following inverse programming problem aiming on the determination of q_{rake}, q_{flank}, h_i, $i = 1,\ldots,6$. For convenience of the programming the following notations were introduced: $w = w(w_1,\ldots,w_6)$, where $w_1=q_{rake}$, $w_2=q_{flank}$, $w_3=h_1$, $w_4=h_2$, $w_5=h_3=h_4$, $w_6=h_5=h_6$; $u(x,y,t)$ – temperature distribution on $\Omega=\Omega_1\cup\ldots\cup\Omega_6$; (x_i, y_i), $i = 1\ldots8$ – coordinates of the location of thermocouples; $u_i^{\exp}(t)$, $i = 1\ldots8$ – experimental data from the thermocouples; $I = \{1\ldots8\}$ – a set of indexes of thermocouples; $[0, T]$ – time interval for both the modeling and the experiments.

Then, the objective function can be written as:

$$f(w) = \max_{(i,t)\in I\times T}\left(u_i^{\exp}(t) - u(x_i, y_i, t, w)\right)^2 \to \min.$$

The upper and lower limits of the parameters w define the feasible set of values: $w_i^{\min} \le w_i \le w_i^{\max}$.

The obtained optimization problem is classified as a constrained type of a problem. It is possible to reduce it to an unconditional optimization problem with the help of a penalty function. The following penalty function is introduced:

$$p(w,z) = \sum_{i=1}^{6}\left[\exp\left(z\left(w_i - w_i^{\max}\right)\right) + \exp\left(z\left(w_i^{\min} - w_i\right)\right)\right],$$

where z - penalty parameter.

Now $w \in \mathbb{R}^6$, where $\mathbb{R}^6$ - six-dimensional vector space, and the objective function is represented as: $F(w,z) = f(w) + p(w,z) \to \min$.

Because the differential properties of the function $f(w)$ are not studied in this paper, the use was made of the alternating-variable descent method, which does not require the calculation of derivatives of the function $f(w)$ on the optimized parameters. Computational scheme of this method is shown on Fig. 6.

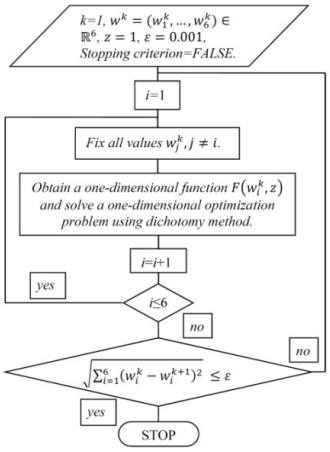

Fig. 6. Computational scheme.

The solution of this inverse problem of minimization of the difference between the experimental and model parameters allows the estimation of heat fluxes on the tool surfaces and respective heat transfer coefficients with the environment. Having these model parameters established, it is possible to calculate the temperature distribution in the tool and its evolution in the course of machining and respective tool wear.

4. Results

Fig. 7 shows the readings from several thermocouples obtained in the machining process. It can be seen that the difference between the temperatures for BCBN and CBN500 tools on TC8 exceeds 100 ºC, and is slightly smaller for other thermocouples. This is related to the difference in the thermal conductivity k of the PCBN grades, where BCBN has almost double the conductivity of CBN500.

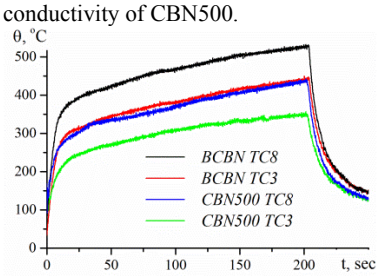

Fig. 7. Examples of temperature readings on thermocouples TC8 and TC3.

The optimized value of the objective function, i.e. the maximum of the mismatch between the model and the experiment over the entire time of the temperature measurement for all thermocouples, equaled 37 ºC and 34 ºC for BCBN and CBN500 tools correspondingly. Fig. 8 shows that while for some of the thermocouples the model overestimates the temperature in the respective positions, for others it might underestimate it. This is most likely related to the limitations of the simplification associated with the use of 2-D model.

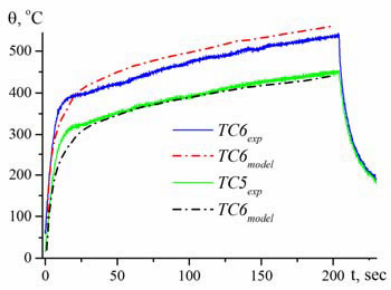

Fig. 8. Comparison of several model and experimental readings on thermocouples installed on BCBN tool.

The values of the q_i and h_i parameters found for the conditions of minimum mismatch are listed in Table 3. Heat transfer coefficients determined for one case of machining were fixed for other PCBN grade because the setup involving the machine tool, toolholder clamping and the holder itself were kept unchanged during experiments and only PCBN inserts were replaced. Therefore only fluxes q_{rake} and q_{flank} were selected as parameters when computing the model for another tool grade. The values of the fluxes are in good agreement with value obtained by other methods [13]. It is also seen that the heat flux through the rake is lower for CBN500 than for BCBN tools. This is consistent with results of [23, 24] showing that the heat partition coefficient β_1 (Fig. 3), i.e. the portion of the friction heat generated on the rake and transmitted into the tool, reduces with the reduced thermal conductivity of a tool material, meaning that higher fraction of the heat will be left in a chip. It is also seen (Table 3) that the flux on the flank, on the opposite, increases for CBN500. This can be related to a possibility of increased heat transfer from the primary shear zone to the workpiece and thus to the tertiary zone as $\eta_1 \cdot P_1$ (Fig. 3) as a result of increased chip temperature.

Table 3. Estimated values of the heat fluxes and heat transfer numbers.

PCBN grade	q_{rake}, W/mm^2	q_{flank}, W/mm^2	h_1, $W/(m^2K)$	h_2, $W/(m^2K)$	h_3, h_4, $W/(m^2K)$	h_5, h_6, $W/(m^2K)$
BCBN	51.8	13.6	8.74	6.13	8.43	5.3
CBN500	39.2	18.1	8.74	6.13	8.43	5.3

Fig 9 shows that the temperature in the steel part of the toolholder practically does not exceed 350 ºC. This means that the maximum local reduction of thermal conductivity k is below 7 % and an increase in the specific heat C_p is below 6%. At the same time thermal diffusivity $\alpha=k/(\rho \cdot C_p)$ changes only by 1 %, which justifies the selection of a linear model for the steel shaft.

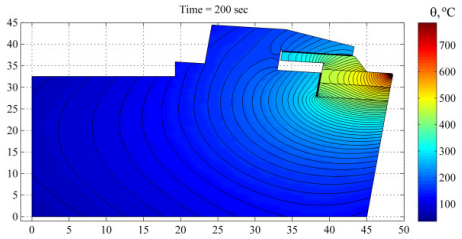

Fig. 9. Temperature field in the toolholder with BCBN insert at VB=0.43 mm.

The maximum temperature developing on the tool in the course of machining and tool wear is presented on Fig. 10. It is seen that upon stabilization within 25-30 seconds the maximum tool temperature attains the value of $\theta_{max} \approx 590$ ºC and continues to increase linearly with the tool wear progression up to $\theta_{max} \approx 780$ ºC. Only a small difference in the maximum temperature is observed between the two PCBN grades. θ_{max} = 776 ºC and θ_{max} = 794 ºC are achieved at the end of tool life for BCBN and CBN500 respectively. Somewhat higher temperatures were measured with IR-CCD technique when hard turning PM tool steels [6], however more aggressive cutting conditions, in terms of cutting speed, and PCBN grade with lower k were applied.

However, even under this close θ_{max}, the difference in the temperature field developing on PCBN grades having different thermal conductivity is very significant. Fig. 11.a, for BCBN grade having k=190 W/m·K, shows that a more uniform temperature field is developed. The maximum temperature is observed in the middle of tool-chip contact. For CBN500 having k=110 W/m·K (Fig. 11.b), the thermal gradient observed in the tool are much higher. Additionally, the maximum temperature is located closer to edge line, which should affect the depth, shape and location of the crater developing on the tool rake. It can be seen that for these PCBN grades having high thermal conductivity a communication between the rake and the flank of the tool is established which enables discussion of average or composite temperature [25]. Observation of the crater on the worn tools with the help of 3-D microscopy (Fig. 12) has revealed that the crater depth equals KT = 89 μm and KT = 129 μm for BCBN and CBN500 grades respectively, even though the flank wear is identical for both grades – VB = 0.43 mm.

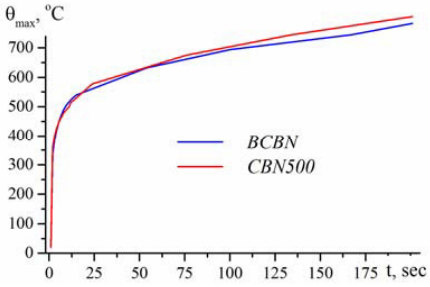

Fig. 10. Development of the maximum tool temperature in the course of machining and tool wear.

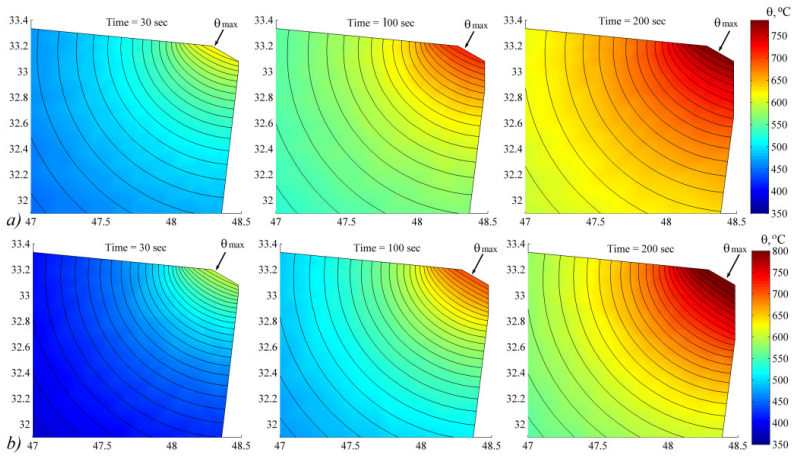

Fig. 11. Temperature field in (a) BCBN and (b) CBN500 inserts at different engagement time and respective tool wear.

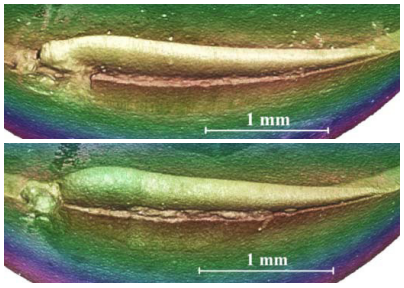

Fig. 12. 3-D view of the worn (a) BCBN and (b) CBN500 tools.

Apart from the KT value itself, it is seen (Fig. 12) that the crater shape for BCBN is more flat than for CBN500 grade. This leads to the development of a more positive geometry on the tool in the course of the wear for CBN500 and thus to the tool weakening. As a result, significantly higher degree of edge chipping and fracture is observed for this grade.

5. Conclusion

A complex FEM-experimental method for the reconstruction of temperature fields developing in a cutting tool in the course of machining and the respective tool wear is developed in the article. The inverse problem aimed on the determination of the heat fluxes on the tool rake and flank faces, as well as heat transfer coefficients was solved by the developed parametric representation of FE model. The experiments and modelling were done for the case of rough dry hard turning of PM tool steel machined with two PCBN grades having different thermal conductivity. The maximum tool temperature was shown to attain the value of $\theta_{max}\approx$590 ºC under new-tool conditions which linearly increased with the tool wear progression up to $\theta_{max}\approx$780 ºC. Only a small difference of ≈ 20 ºC between θ_{max} was found for PCBN grades with various thermal conductivities k. This was found to be related to the reduction of the heat flux on the rake for a PCBN grade with lower k. Temperature fields, on the other hand, varied significantly, with θ_{max} being located closer to the edge line for the PCBN grade having lower k. The θ_{max} and the temperature distribution for the PCBN tools were found to accurately reflect the crater wear observed on the respective tools.

Acknowledgements

This work has been done as a part of the research project Sustainable Production Initiative (SPI). The support of SECO Tools AB and Uddeholm Tooling AB is greatly appreciated. The authors sincerely thank L. Siesing (Lund University) for the help with thermal conductivity measurement. The cooperation research initiative between Institute for Superhard Materials (Ukraine) and Lund University (Sweden) is also greatly acknowledged.

References

[1] Davies MA, et al. On the measurement of temperature in material removal processes. CIRP Ann 2007; 56:581-604.
[2] Sumiya H, Uesaka S, Satoh S. Mechanical properties of high purity polycrystalline cBN synthesized by direct conversion sintering method. J Mater Sci 2000; 35:1181-1186.
[3] M'Saoubi R, Johansson MP, Andersson JM. Wear mechanisms of PVD-coated PCBN cutting tools. Wear 2013; 302:1219-1229.
[4] Bushlya V, et al. Effects of cutting speed when turning age hardened Inconel 718 with PCBN tools of binderless and low-cBN grades. Mach Sci Technol 2013; 17:497–523.
[5] Bushlya VM, et al. Tool wear and tool life of PCBN, binderless cBN and wBN-cBN tools in continuous finish hard turning of cold work tool steel. J Superhard Mater+ 2014; 36:49-60.
[6] Stephenson DA. Tool-work thermocouple temperature measurements - theory and implementation issues. J Eng Ind-T ASME 1993; 115:432-437.
[7] Ueda T, Sato M, Hosokawa A, Ozawa M. Development of infrared radiation pyrometer with optical fibers-Two-color pyrometer with non-contact fiber coupler. CIRP Ann - Manuf Techn 2008; 57:69-72.
[8] Hosseini SB, Beno T, Klement U, Kaminski J, Ryttberg K. Cutting temperatures during hard turning - Measurements and effects on white layer formation in AISI 52100. J Mater Process Technol 2014; 214:1293-1300.
[9] M'Saoubi R, Lebrun JL, Changeux B. A new method for cutting tool temperature measurement using CCD-infrared technique: Influence of tool and coating. Mach Sci Technol 1998; 2:369-382.
[10] M'Saoubi R, et al. Machinability of powder metallurgy steels using PcBN inserts. Procedia CIRP 2014; 14:83-88.

[11] Ren XJ, et al. Cutting temperatures in hard turning chromium hardfacings with PCBN tooling. J Mater Process Tech 2004; 147:38-44.
[12] El-Wardany TI, Mohammed E, Elbestawi MA. Cutting temperature of ceramic tools in high speed machining of difficult-to-cut materials. Int J Mach Tool Manu 1996; 36/5:611-634.
[13] Norouzifard V, Hamedi M. Experimental determination of the tool – chip thermal contact conductance in machining process. Int J Mach Tool Manu 2014; 84:45-57.
[14] Stahl J-E. Metal cutting: theories and models. Fagersta: SECO Tools; 2012.
[15] Isaev KB, et al. Determination of the thermal conductivity coefficient of superhard materials. Powder Metall Met C+ 2003; 42:310-314.
[16] Makedon ID, Petrov AV, Feldgun LI. Thermal conductivity of compacts of cubic BN. Izv Akad Nauk SSSR: Inorg Chem 1972; 8/2:765-766.
[17] Primachuk VL, et al. Thermo-physical properties of various modifications of boron nitride. Powder Metall Met C+ 1983; 8:80-82.
[18] Phase and structural transformations of pyrolytic boron nitride at high pressure. Dr.Sc. Thesis. Institute for Superhard Materials, Ukraine, 2002.
[19] Chernikova ES, et al. An analysis of electric heating of a cemented carbide taking into consideration the temperature relationship of its characteristics. Powder Metall Met C+ 1992; 31:936-940.
[20] Barrow G, Graham W, Kurimoto T, Leong YF. Determination of rake face stress distribution in orthogonal machining. Int J Mach Tool D R 1982; 22:75-85.
[21] Yvonnet J, Umbrello D, Chinesta F, Micari F. A simple inverse procedure to determine heat flux on the tool in orthogonal cutting. Int J Mach Tool Manu 2006; 46:820-827.
[22] Zhou JM, Walter H, Andersson M, Stahl JE. Effect of chamfer angle on wear of PCBN cutting tool. Int J Mach Tool Manu 2003; 43:301–305.
[23] Kagnaya T, et al. Temperature evolution in a WC-6%Co cutting tool during turning machining: Experiment and finite element simulations. WSEAS Trans HAMT 2011; 6:71-80.
[24] Shaw MC. Metal cutting principles. 2nd ed. Oxford: Oxford University Press; 2004.
[25] Stahl JE. Modelling of the composite temperature θc in metal cutting tools. J Superhard Mater+ 2015; accepted for publication.